

COVER PAGE

Document downloaded by @DAEL

Thu Nov 26 23:17:33 2026
For personal use

When automatic English translation is provided, only the original document is authentic.
The EAA cannot be held responsible of any translation error

Bibliographical reference

An Improved Tubular Ultrasonic Radiator in Longitudinal and Radial Composite Vibration, Long Xu and Shuyu Lin, Acta Acustica **vol. 101** (Number 1), 2015, pp. 37-45

DOI
https://doi.org/10.3813/AAA.918802

Acta Acustica united with Acustica
Vol. 101 (2015) 37 – 45

DOI 10.3813/AAA.918802

An Improved Tubular Ultrasonic Radiator in Longitudinal and Radial Composite Vibration

Long Xu[1)], Shuyu Lin[2)]

[1)] Department of Physics, China Jiliang University, Hangzhou 310018, China.
xulong250864@163.com, xulong@cjlu.edu.cn

[2)] Institute of Applied Acoustics, Shaanxi Normal University, Xi'an 710062, China

Summary

An improved tubular ultrasonic radiator was proposed and studied. It is composed of a sandwich piezoelectric transducer working in a longitudinal vibration mode, of a barbell horn, which used as the displacement and cross-section amplifier to amplify both the longitudinal displacement amplitude and the output cross-section of the transducer, and of a long metal tube that is designed to vibrate in fundamental radial vibration mode at the same working frequency of the sandwich piezoelectric transducer. With structural optimization and vibrational mode conversion, the improved tubular ultrasonic radiator can effectively transform the longitudinal vibration excited by the transducer into the intense radial vibration of the long metal tube. The electro-mechanical equivalent circuit for the longitudinal and radial composite vibration of the radiator was given. The composite vibrational modes and the radiated sound field of the radiator were simulated and analyzed. The resonance frequency, the impedance-frequency curves and the vibrational displacement distribution were numerically simulated and experimentally measured. It is experimentally shown that the measured results are in agreement with the analytical and numerical results, and that the strong radial vibration of the radiator can be excited by the longitudinal vibration of the sandwich longitudinal piezoelectric transducer. Therefore, it is expected to be used as high power ultrasonic radiators in ultrasonic cleaning, ultrasonic extraction, ultrasonic liquid processing and ultrasonic sonochemistry.

PACS no. 43.35.-c, 43.38.-p

1. Introduction

Along with the development of high power ultrasonic technology, such as in large volume ultrasonic cleaning, ultrasonic sewage treatment, Chinese herbal medicine extraction and ultrasonic sonochemistry, high displacement ultrasonic transducers and radiators with large radiating surfaces and powers are needed increasingly. In order to improve the vibration performance for the ultrasonic vibration system, many scholars and engineers have been doing a lot of works in this field. The stepped-plate directional HPU transducers, a very useful type of transducers for the generation of ultrasounds in fluids, have already been commercialized and applied industrially [1, 2, 3]. A new HPU vibration system which is excited by several transducers has been presented [4]. Peshkovsky et al. [5, 6, 7, 8] presented a new ultrasonic rod waveguide-radiator, and gave the design principles of the waveguide-radiator, including the equations and expressions for displacements, strains and gain factor. In their work, the conical-cylindrical, stepped, barrel, spool-shaped and barbell-shaped horns were discussed. Different from the other horns, the barbell horn operated in the full-wave vibrational mode has a large radiating surface and high gain factor. Their experiments also supported that the barbell horn was more suitable for the liquid processing. Dahlem et al. [9] proposed the radially vibrating horn, which can give radiation in longitudinal and radial directions. A kind of HPU cylindrical transducers with frequency of 20 kHz and power capacities from 500W to 16000W, produced by the Hielscher Ultrasonics GmbH from Germany, have also been commercialized and industrially applied [10].

In recent years, to increase the output power for a single transducer, tubular ultrasonic radiators have been presented and used. A push-pull transducer with a high power capacity of 2000W has been produced by the Crest Ultrasonics Corp. from America [11]. Both the resonance and radiated sound characteristics of the push-pull transducers have been investigated by some Chinese scholars [12, 13]. According to their analytical results, due to the tubular radiators designed in the higher radial-flexural vibration mode, the distribution of the radial ultrasound field for this type of transducers is uneven. Lin ea al. proposed a new type of high power composite ultrasonic transducer [14]. Although it can improve performance of the radiating sound for the tubular radiators, the radial vibration of the transducer is weaker than its longitudinal vibration.

In this paper, in order to further improve the radial vibration performance for the tubular transducer, an im-

Received 15 April 2013,
accepted 05 July 2014.

© S. Hirzel Verlag · EAA

proved tubular ultrasonic radiator with large radiating area is proposed and investigated. It is composed of a sandwich piezoelectric transducer working in a longitudinal vibration mode, of a barbell horn [5, 6, 7, 8], which used as the displacement and cross-section amplifier to amplify both the longitudinal displacement amplitude and the output cross-section of the transducer, and of a long metal tube that is designed to vibrate in fundamental radial vibration mode at the same working frequency of the sandwich piezoelectric transducer. By virtue of structural optimization and vibration mode conversion, the longitudinal vibration excited by the transducer can be efficiently amplified by the barbell horn, and then be converted to the intense radial vibration of the long metal tube by virtue of vibrational mode conversion. So the high intensity ultrasound can be produced all around the outer surface of the radiator.

In the following analysis, the electro-mechanical equivalent circuit of the improved tubular ultrasonic radiator was given, and then the input mechanical reactance spectrum was obtained analytically. To verify the analytical theory and results, numerical method was also used to simulate the vibrational characteristics of the radiator. And the vibrational mode, the longitudinal and radial vibrational displacement distribution, the impedance-frequency curve, and the radiated sound field were given. Finally, the improved tubular ultrasonic radiator was designed and manufactured; its resonance frequency and impedance-frequency curve were measured experimentally by using Agilent 4294A Precision Impedance Analyzer, and its radial vibrational displacement distribution was measured and observed by using Polytec PSV-400 Scanning Vibrometer.

2. Working principle

Figure 1 shows the proposed improved tubular ultrasonic radiator: it is composed of a sandwich piezoelectric transducer working in a longitudinal vibration mode, of a barbell horn, which used as the displacement and cross-section amplifier to amplify both the longitudinal displacement amplitude and the output cross-section of the transducer [5], and of a long metal tube that is designed to vibrate in fundamental radial vibration mode at the same working frequency of the sandwich piezoelectric transducer. Once the sandwich longitudinal transducer and the barbell horn are excited to vibrate longitudinally, the radial fundamental resonant mode of the long metal tube is also excited by virtue of vibration mode conversion at the same frequency. Since the barbell horn is able to efficiently amplify both the longitudinal vibration displacement and the output cross-section of the transducer, the long metal tube can receive more intensely excited displacement, and its radial dimension can be designed much larger than that of the transducer. Therefore, by virtue of the special structure designation and the vibration mode conversion, it can effectively improve the ultrasonic radiating area and intensity of the radiator.

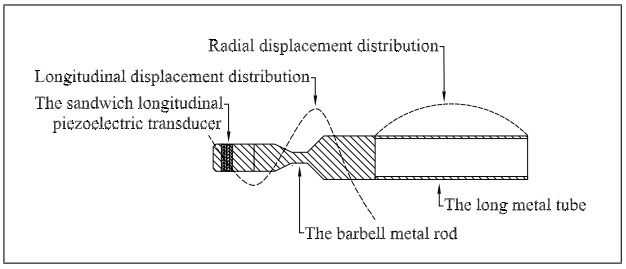


Figure 1. Schematic diagram of the improved tubular ultrasonic radiator.

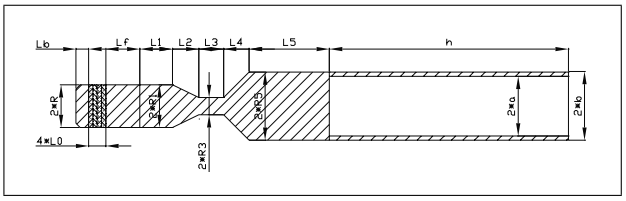


Figure 2. Geometrical diagram of the improved tubular ultrasonic radiator.

3. Analysis of the improved tubular ultrasonic radiator in longitudinal and radial composite vibration

The geometrical diagram of the improved tubular ultrasonic radiator is shown in Figure 2. In the figure, L_b and L_f are the lengths of the back and front metal masses in the sandwich longitudinal piezoelectric transducer, whose radii are both equal to R. In the sandwich longitudinal piezoelectric transducer, there are p identical piezoelectric ceramic elements, with the thickness of L_0 for each element. In general, p is a positive even number, and the piezoelectric ceramic elements are ring-shaped. The barbell horn is composed of five elements: the first cylindrical element, the second conical element, the third cylindrical element, the fourth conical element and the fifth cylindrical element. Their lengths are denoted as L_1, L_2, L_3, L_4 and L_5, respectively. The radii of the first, the third and the fifth cylindrical elements are R_1, R_3 and R_5, respectively. h is the height of the long metal tube, whose inner and outer radii are a and b.

The electro-mechanical equivalent circuit model has been proven to be very useful in designing and analyzing the vibrational characteristics of elastic mechanical elements. The sandwich longitudinal piezoelectric transducer, one component of the radiator, has already been studied extensively, and its design method is well known. Therefore, only the electro-mechanical equivalent circuit and resonance frequency equations of the barbell horn and the long metal tube are given here.

The barbell horn consists of five elements, including three constant cross-section cylinders and two conical cross-section rods connected in series mechanically. According to the equivalent circuits of a conical metal rod and a constant cross-section metal rod, the equivalent circuit of the five-element barbell horn can be obtained as is

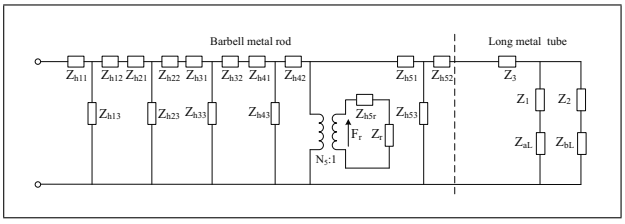


Figure 3. The electro-mechanical equivalent circuit for the combination of the barbell horn and the long metal tube.

shown in the left of the dot line in Figure 3. In the figure, Z_{h11}, Z_{h12}, Z_{h13}, Z_{h21}, Z_{h22}, Z_{h23}, Z_{h31}, Z_{h32}, Z_{h33}, Z_{h41}, Z_{h42}, Z_{h43} are the mechanical impedances for the first cylindrical element, the second conical element, the third cylindrical element, the fourth conical element in the barbell horn; for the radial dimension of the fifth cylindrical element of the barbell horn being designed to be larger than a quarter of the longitudinal wavelength, the radial coupled vibration of the fifth cylindrical element of the barbell horn should be taken into account, and these two vibrations are coupled together by means of the mechanical conversion N_5 ($N_5 = nR_5/2L_5$) [15]. So the mechanical impedances of the fifth cylindrical element of the barbell horn are composed of equivalent longitudinal vibration mechanical impedances Z_{h51}, Z_{h52}, Z_{h53} and equivalent radial vibration mechanical impedance Z_{h5r}. While, $S_{h1} = \pi R_1^2$, $S_{h3} = \pi R_3^2$ and $S_{h5} = \pi R_5^2$ are respectively the cross-sectional areas for the first cylindrical element, the third cylindrical element and the fifth cylindrical element of the barbell horn, and $S_{h5r} = 2\pi R_5 l_5$ is the area of lateral surface of the fifth cylindrical element of the barbell horn. $c_z = \sqrt{E_z/\rho}$ and $c_r = \sqrt{E_r/\rho}$ are sound speed of the equivalent longitudinal vibration and the equivalent radial vibration. $E_z = E(1+2\nu)/n)^{-1}$ and $E_r = E[1-\nu^2+n\nu(1+\nu)]^{-1}$ are the longitudinal and radial equivalent elastic constants; $k_z = \omega/c_z$ and $k_r = \omega/c_r$ are the equivalent longitudinal and radial wavenumbers. ρ, E, ν and c are volume density, Young's modulus, Poisson's ratio and sound speed of the longitudinal vibration.

In general cases, the vibration for a metal tube is a coupled one, and its analytical solutions are difficult to find. In the manuscript, it is assumed that the length h of the metal tube is much larger than its radius b, i.e. $h \gg b$. In this case, the vibration of the long metal tube can be reduced to a problem of plane strain, and the corresponding wave equations can be obtained [16],

$$\frac{\mathrm{d}^2\xi_{r0}}{\mathrm{d}r^2} + \frac{1}{r}\frac{\mathrm{d}\xi_{r0}}{\mathrm{d}r} + \left(k^2 - \frac{1}{r^2}\right)\xi_{r0} = 0. \tag{1}$$

The solution to equation (1) can be expressed by

$$\xi_r(r,t) = \left[A_1 J_1(kr) + A_2 Y_1(kr)\right] \exp\left(\mathrm{j}\omega t\right). \tag{2}$$

Here, $J_1(kr)$ and $Y_1(kr)$ are Bessel functions of order one, A_1 and A_2 are two constants, they can be determined by the boundary conditions.

From equation (2), the radial vibrational velocity can be obtained,

$$v_r = \mathrm{j}\omega\left[A_1 J_1(kr) + A_2 Y_1(kr)\right]\mathrm{e}^{\mathrm{j}\omega t}. \tag{3}$$

From Figure 2, when $r = a$, $v_r = v_a$; when $r = b$, $v_r = -v_b$. Therefore, the constants A_1 and A_2 can be obtained as

$$A_1 = -\frac{\mathrm{j}Y_1(kb)}{\Delta\omega}v_a - \frac{\mathrm{j}Y_1(ka)}{\Delta\omega}v_b, \tag{4}$$

$$A_2 = -\frac{\mathrm{j}J_1(kb)}{\Delta\omega}v_a - \frac{\mathrm{j}J_1(ka)}{\Delta\omega}v_b. \tag{5}$$

Here, $\Delta = J_1(ka)Y_1(kb) - J_1(kb)Y_1(ka)$. From Figure 2, the boundary conditions for radial forces can be expressed as

$$F_a = -\frac{\mathrm{j}Z_{01}}{k}\left[\left(\frac{\Delta_1}{\Delta} + \frac{n_1}{n_2 a}\right)v_a + \frac{2}{\Delta a\pi}v_b\right], \tag{6}$$

$$F_b = -\frac{\mathrm{j}Z_{02}}{k}\left[\frac{2}{\Delta b\pi}v_a + \left(\frac{\Delta_2}{\Delta} + \frac{n_1}{n_2 b}\right)v_b\right]. \tag{7}$$

Here, $Z_{01} = \rho S_a v$, $Z_{02} = \rho S_b v$, $\Delta_1 = J_1(kb)Y_1'(ka) - J_1'(ka)Y_1(kb)$, $\Delta_2 = J_1(ka)Y_1'(kb) - J_1'(kb)Y_1(ka)$. $S_a(= 2\pi ah)$ and $S_b(= 2\pi bh)$ are inner and outer side areas of the metal tube, $k = \omega/c$, k is wave number, ω is angular frequency, $v^2 = E/(\rho n_1)$, $n_1 = (1+\sigma)(1-2\sigma)/(1-\sigma)$, $n_2 = (1+\sigma)(1-2\sigma)/\sigma$, v is sound speed of radial vibration in a long metal tube, ρ, E and σ are volume density, Young's modulus and Poisson's ratio. Using equations (6) and (7), the electro-mechanical equivalent circuit for a metal long tube in radial vibration can be obtained as is shown in the right of the dot line in Figure 3. In the figure, the impedances for the series and parallel arms can be obtained as the following forms,

$$Z_1 = -\frac{\mathrm{j}Z_{01}}{k}\left(\frac{\Delta_1}{\Delta} - \frac{n_1}{n_2 a} - \frac{2}{\Delta a\pi}\right), \tag{8}$$

$$Z_2 = -\frac{\mathrm{j}Z_{02}}{k}\left(\frac{\Delta_2}{\Delta} - \frac{n_1}{n_2 b} - \frac{2}{\Delta b\pi}\right), \tag{9}$$

$$Z_3 = -\frac{2\mathrm{j}Z_{01}}{\Delta ka\pi} = -\frac{2\mathrm{j}Z_{02}}{\Delta kb\pi}. \tag{10}$$

Z_{aL} and Z_{bL} are load mechanical impedances of the radiator at its inner and outer surfaces. In the paper, the radiator is used as an immersed ultrasonic radiator which ultrasound is emitted radially from the outside of the radiator. Therefore, the inner surface of the radiator is air-backed and Z_{aL} can be regarded as zero. The outer surface of the metal tube is contacted with load medium which determines the load impedance Z_{bL}. It is well-known that the load impedance Z_{bL} is dependable on the working frequency, the geometrical dimension of the radiator, and the load medium, whose analytical expressions is difficult to be given. Therefore, it is usually ignored in the engineering design of the radiator by letting Z_{bL} be zero.

From Figure 3, once the material parameters and the geometrical dimensions of the barbell horn and the long metal tube are given, the input mechanical impedance of the combination of the barbell horn and the long metal tube (Z_r) can be obtained by using the transmission lines impedance transfer formula, and its resonance frequency equation can be obtained when the reactance of Z_r is set to zero. Figure 4 shows the input mechanical reactance spectrum of the combination of the barbell horn and the long

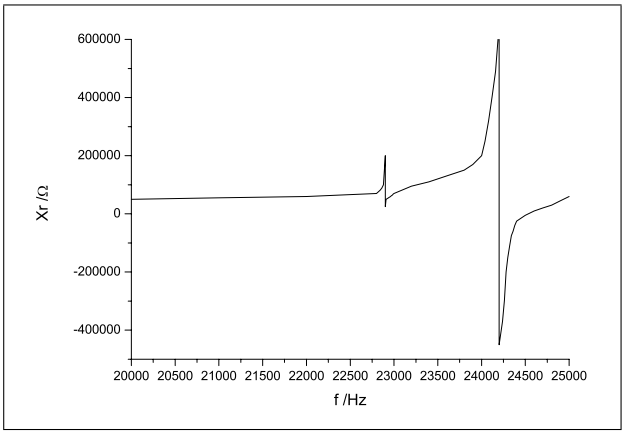


Figure 4. The input mechanical reactance spectrum of the combination of the barbell horn and the long metal tube.

metal tube. It can be seen from Figure 8 that there are two resonance peaks in the calculated frequency range (from 20 to 25 kHz). And it is should be noted that the first resonance peak corresponds to the designed operation mode of the radiator.

4. Numerical analysis and experimental demonstration

In the above analysis, the longitudinal and radial composite vibration of the radiator was analytically studied and the input mechanical reactance spectrum is obtained using the electro-mechanical equivalent circuit method. For comparison, numerical method was further used to simulate the longitudinal and radial composite vibration, and some experimental results were also given in the following section.

4.1. Numerical analysis

It is well known that the numerical method is a useful tool in the analysis of complex vibration systems. It can give the vibrational modal shape, the natural frequency, the electro-mechanical impedance curve and radiated sound field of the vibrational system [17, 18]. In this section, the ANSYS program was used to simulate the longitudinal and radial composite vibration of the improved tubular ultrasonic radiator. The geometrical dimensions of the radiator are listed in Table I. As the radiator is an axisymmetric structure, it can be represented by a plane (2D) finite element model. The element types and material properties for simulating each part of the radiator are as follows: the long metal tube and the barbell horn are simulated by axial symmetric plane element (plane 42); the type of metal for the tube and barbell horn is 45# steel, its standard material parameters are density $\rho_s = 7840\,\mathrm{kg/m^3}$, Young's modulus $E_s = 2.16 \cdot 10^{11}\,\mathrm{N/m^2}$, Poisson ratio $\sigma_s = 0.28$; the front and back metal mass in the sandwich longitudinal transducer are simulated by axial symmetric plane element (plane 42) and their material parameters are $\rho_A = 2790\,\mathrm{kg/m^3}$, $E_A = 7.15 \cdot 10^{10}\,\mathrm{N/m^2}$, $\sigma_A = 0.34$; the

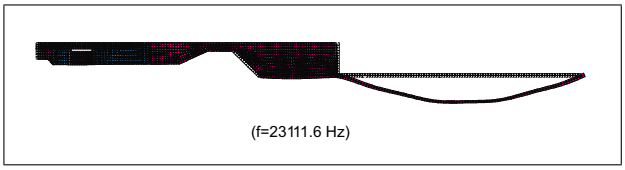


Figure 5. Numerically simulated modal shape of the radiator in the composite vibration.

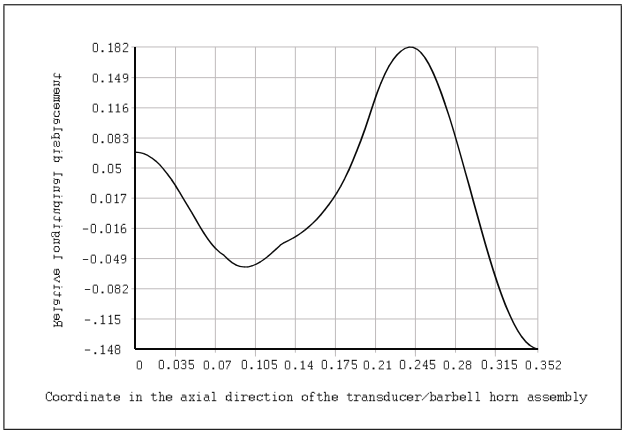


Figure 6. Numerically simulated longitudinal vibrational displacement distribution in the part of the transducer and barbell horn for the radiator in its composite vibration.

piezoelectric elements (PZT-4) in the sandwich longitudinal transducer are simulated by axial symmetric plane element (plane 13) and their standard material parameters are $\rho_0 = 7500\,\mathrm{kg/m^3}$, $s_{11}^E = 12.3 \cdot 10^{-12}\,\mathrm{m^2/N}$, $s_{12}^E = -4.05 \cdot 10^{-12}\,\mathrm{m^2/N}$, $s_{33}^E = 15.5 \cdot 10^{-12}\,\mathrm{m^2/N}$, $v_{12}^E = 0.33$, $d_{31}^E = -123 \cdot 10^{-12}\,\mathrm{C/N}$, $d_{33}^E = 289 \cdot 10^{-12}\,\mathrm{C/N}$, $d_{15}^E = 496 \cdot 10^{-12}\,\mathrm{C/N}$, $\varepsilon_{33}^T/\varepsilon_0 = 1300$, $\varepsilon_0 = 8.842 \cdot 10^{-12}\,\mathrm{F/m}$. In calculating the radiated sound of the improved tubular ultrasonic radiator, water is chosen as the medium. The water out of the long metal tube is simulated by the acoustic element (fluid 29) and its density $\rho_w = 1000\,\mathrm{kg/m^3}$, sound velocity $v_w = 1500\,\mathrm{m/s}$.

The vibrational modal shapes and the displacement amplitude distribution of the radiator can be obtained by the modal analysis from ANSYS program. Figure 5 is the numerically simulated modal shape of the radiator in the composite vibration. It can be seen from Figure 5 that the longitudinal vibration, which is excited from the sandwich piezoelectric transducer and then be amplified by the barbell metal tube, can be efficiently translated into the radial vibration of the long metal tube. In order to inspect the displacement amplitude for each part of the radiator in its longitudinal and radial composite vibration, the longitudinal vibrational displacement distributions for the transducer and barbell horn on their axial directions are simulated (shown in Figure 6), meanwhile, the vibrational displacement distributions for the long metal tube on its side surface are also simulated (shown in Figure 7). From Figure 6, it can be seen that the longitudinal displacement amplitude of the sandwich piezoelectric transducer can be efficiently amplified by the barbell metal tube, so the in-

Table I. Geometrical dimensions (in mm) of the radiator.

L_1	L_2	L_3	L_4	L_5	R_1	R_3	R_5	a	b	h
38.4	31.4	29.6	30.7	94.0	25.0	10.0	40.0	36.0	40.0	180.0

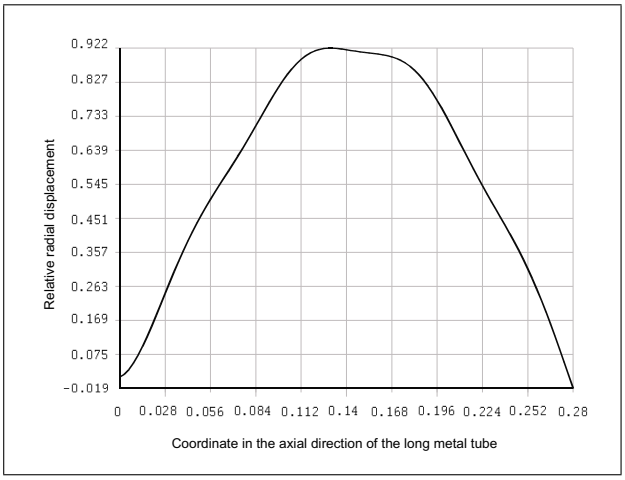


Figure 7. Numerically simulated radial vibrational displacement distribution in the part of the long metal tube for the radiator in its composite vibration.

tense longitudinal vibration can be obtained to excite the long metal tube vibrated in its radial vibration. Figure 7 illustrates the radial displacement distribution for the long metal tube on its side surface. It can be seen that the radial displacement for the long metal tube is not uniform, which illustrates that the radial vibration is strong in the middle and weak at the end of the tube. By comparing Figure 6 with Figure 7, it can be seen that the radial displacements nearing the middle of the tube are much larger than the longitudinal displacements at the output surface of the barbell horn, which means that the longitudinal vibration from the barbell horn is effectively transformed into the more intense radial vibration of the tube. In order to quantitatively describe the conversion efficiency from the longitudinal vibration of the barbell horn to the radial vibration of the long metal tube, the displacement amplitude conversion ratio between the longitudinal and radial vibration is defined as

$$\tau = U_r/U_l. \tag{11}$$

Here, U_r is the maximal relative value of the radial displacement for the long metal tube on its side surface; U_l is the maximal relative value of the longitudinal displacement for the barbell metal tube on its output surface; τ is the displacement amplitude conversion ratio between the longitudinal and radial vibration. From equation (11), it can be seen that the bigger value of τ, the better conversion efficiency from the longitudinal vibration of the barbell horn to the radial vibration of the long metal tube, and vice versa. For the improved tubular ultrasonic radiator studied in this paper, the value of τ is 6.2 (which calculated by the datum from Figures 6 and 7), so it means

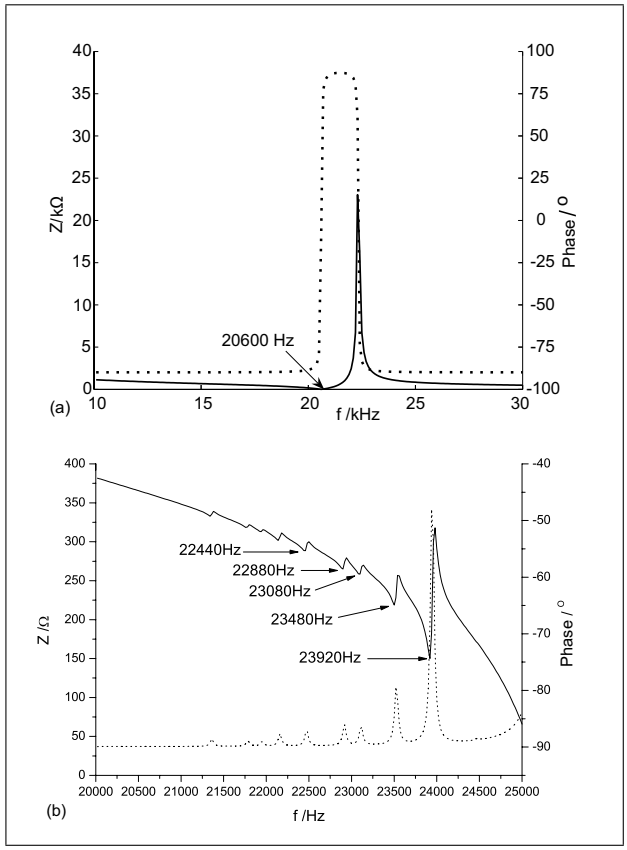


Figure 8. Numerically simulated impedance-frequency curves for the sandwich transducer and the improved tubular ultrasonic radiator: (a) Numerically simulated impedance-frequency curve of the sandwich transducer; (b) Numerically simulated impedance-frequency curve of the improved tubular ultrasonic radiator.

that the radiator has the better conversion efficiency in the process of the longitudinal vibration transforming into the radial vibration.

From the above simulated results, it can conclude that, by virtue of the special structure designation and the vibration mode conversion, it can not only improve the ultrasonic radiation space of the traditional sandwich piezoelectric transducer, but effectively improve its vibrational displacement.

Figure 8 is numerically simulated impedance-frequency curves for the sandwich transducer and the improved tubular ultrasonic radiator. It can be seen that the impedance-frequency curve (b) for the improved tubular ultrasonic radiator becomes complex compared with the impedance-frequency curve (a) for the single sandwich piezoelectric transducer. By comparing Figure 8a with 8b, it can be seen that the value of resonance impedance is much larger, that there are more impedance peaks, and that the band-

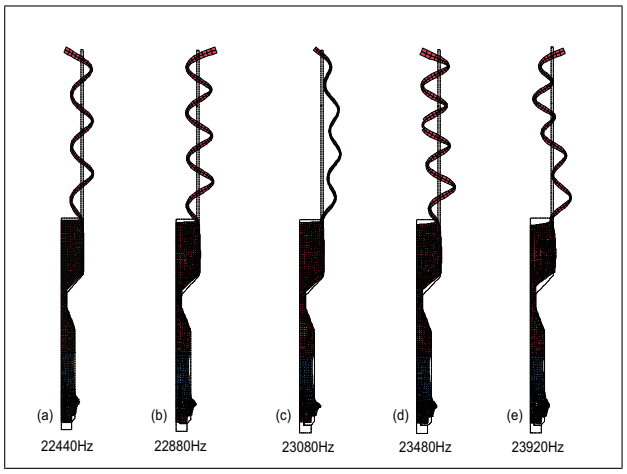


Figure 9. Simulated modal shapes in different vibration mode of the radiator.

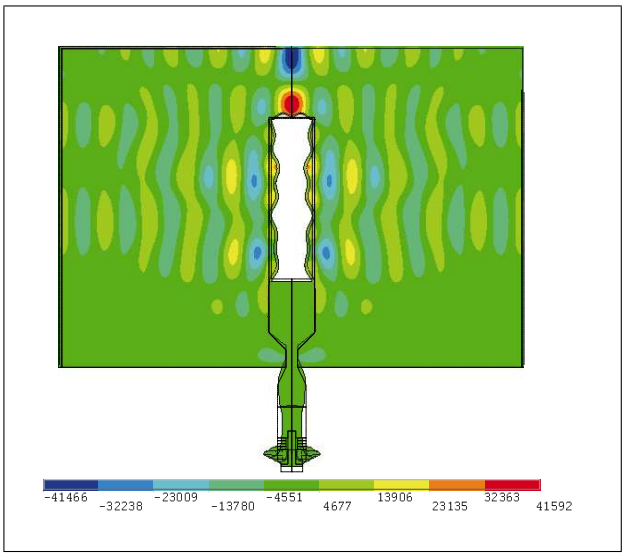


Figure 10. Simulated sound field distribution (real part of the radiated sound pressure) of the radiator in its longitudinal and radial composite vibration.

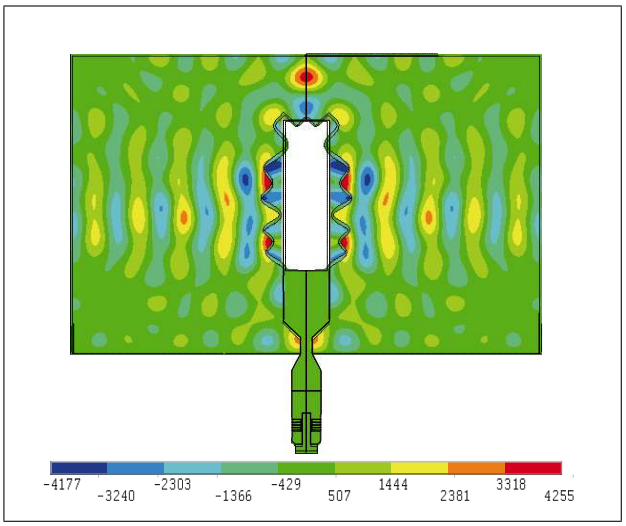


Figure 11. Simulated sound field distribution (imaginary part of the radiated sound pressure) of the radiator in its longitudinal and radial composite vibration.

width becomes narrower at each resonance mode for the improved tubular ultrasonic radiator. The main reason for this phenomenon lies in three aspects. First, the more the contact surfaces between the different vibration elements for the improved tubular ultrasonic radiator (the sandwich transducer, the barbell horn and the metal tube) have, the larger its resonance impedance will be. Second, the interactions of the sandwich transducer, the barbell horn and the metal tube of the improved tubular ultrasonic radiator will lead to some new vibration modes. Third, with the longitudinal dimensions of the whole radiator much larger than that of the single transducer, the vibration modes of the radiator nearing the fundamental resonance frequency of the single sandwich transducer correspond to its different higher harmonic resonance modes, so their bandwidth become much narrower.

Figure 9 illustrates the mode shapes which corresponding to the impedance peaks marked in Figure 8b. In Figure 9, by comparing (c) with (a), (b), (d), (e), it can be seen that apart from the longitudinal and radial composite vibration mode (the designed operation mode at 23080 Hz) of the radiator, the different longitudinal and radial flexural vibration modes are also excited by the longitudinal vibration of the sandwich piezoelectric transducer. So it should be noted that in the practical application the frequency of the ultrasonic generator must be matched exactly with the one of the longitudinal and radial composite vibration mode for the radiator; otherwise, the radiator will operate in the other radial flexural vibration modes, as shown in Figure 9.

Based on the simulated vibrational modal shapes and the impedance-frequency curves of the radiator, the radial radiated sound field is also numerically simulated; water is chosen as the medium. It is simulated by the acoustic element (fluid 29) and its density $\rho_w = 1000\,\mathrm{kg/m^3}$, sound velocity $v_w = 1500\,\mathrm{m/s}$. The numerically simulated radiated sound fields of the radiator in its longitudinal and radial composite vibration mode are illustrated in Figures 10–12. The radiated sound pressure can be represented by the real part or imaginary part of the pressure. Figures 10 and 11 are the real part and the imaginary part of the simulated radiated sound pressure. Generally speaking, if there are significant differences between the real part and the imaginary part of the radiated sound pressure in the near field, it implies that the phase distribution of the radiated sound pressure is very complicated. In this case, only the real part or the imaginary part of the radiated sound pressure are inadequate to describe the radiated pressure distribution, and the absolute value, or the modulus of the radiated sound pressure is needed to describe the distribution of the radiated sound pressure, i.e. the beam pattern of the radiated sound pressure. Figure 12 shows the beam pattern of the sound field while the radiator operates in its longitudinal and radial composite vibration mode. It can be seen

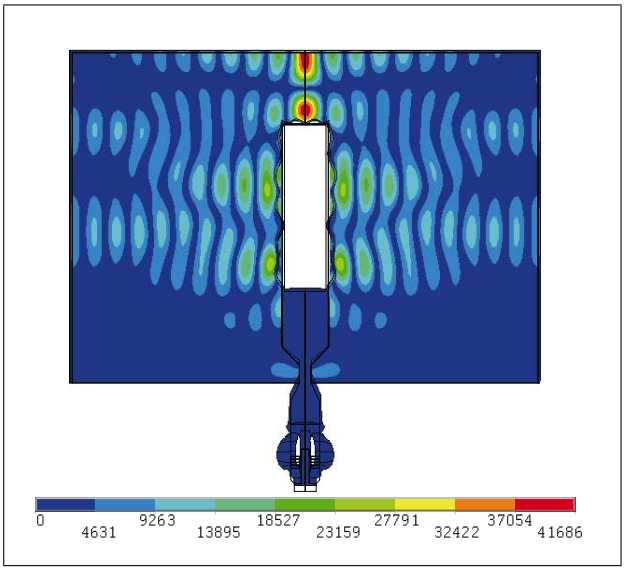


Figure 12. The beam pattern of the radiated sound field (modulus of the radiated sound pressure) of the radiator in its longitudinal and radial composite vibration.

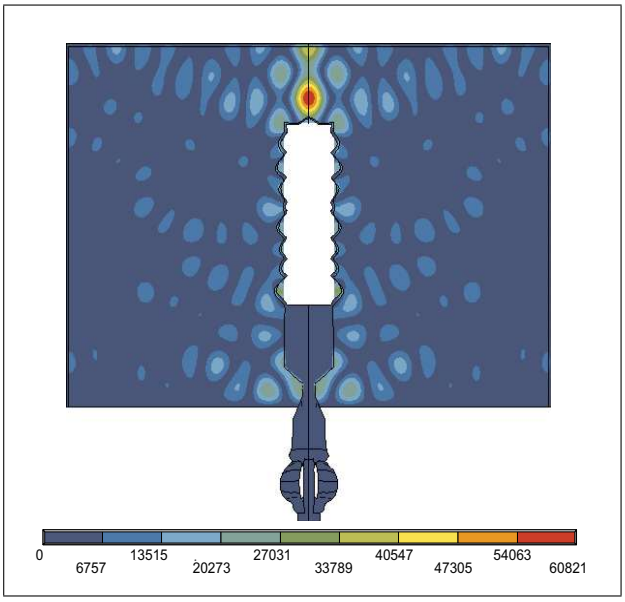


Figure 13. The beam pattern of the radiated sound field (modulus of the radiated sound pressure) of the radiator in its longitudinal and radial flexural composite vibration.

from Figure 12 that ultrasound can be produced around the outer surface of the radiator.

For comparison, a radiated sound field of the radiator in its longitudinal and radial flexural composite vibration mode is also simulated, as is shown in Figure 13. By comparing Figure 13 with Figure 12, it can be seen that the radiated sound field of the radiator in its longitudinal and radial composite vibration mode is much better than the one in the longitudinal and radial flexural composite vibration mode. It is the reason why we choose the longitudinal and radial composite vibration mode of the radiator as its operating vibration mode.



Figure 14. Photograph of the improved tubular ultrasonic radiator.

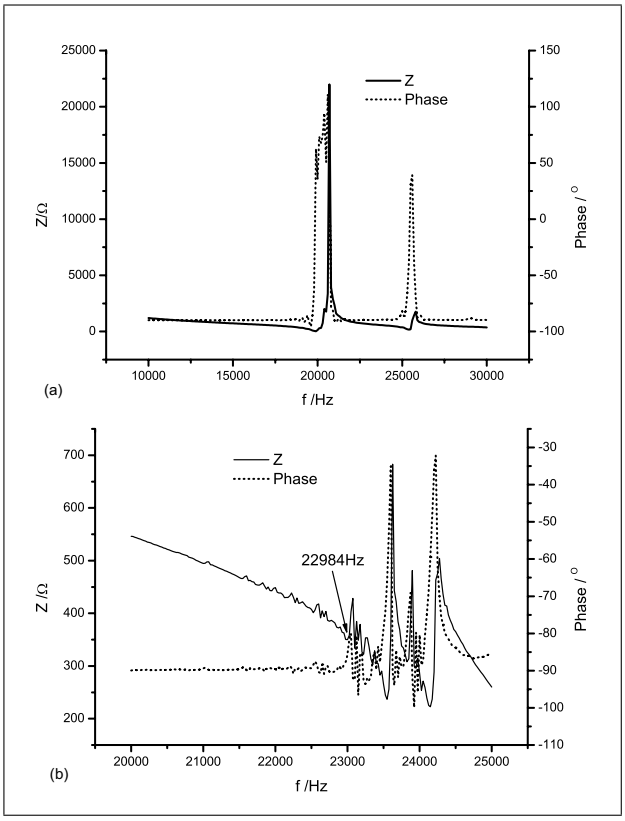


Figure 15. Measured impedance-frequency curves for the sandwich transducer and the improved tubular ultrasonic radiator: (a) Numerically simulated impedance-frequency curve of the sandwich transducer; (b) Numerically simulated impedance-frequency curve of the improved tubular ultrasonic radiator.

4.2. Experiment results

In order to experimentally validate theoretical analysis results, an improved tubular ultrasonic radiator was fabricated (please see Figure 14) and its vibrational performances were measured. First, the impedance-frequency characteristics of the radiator were measured by using Agilent 4294A Precision Impedance Analyzer. Second,

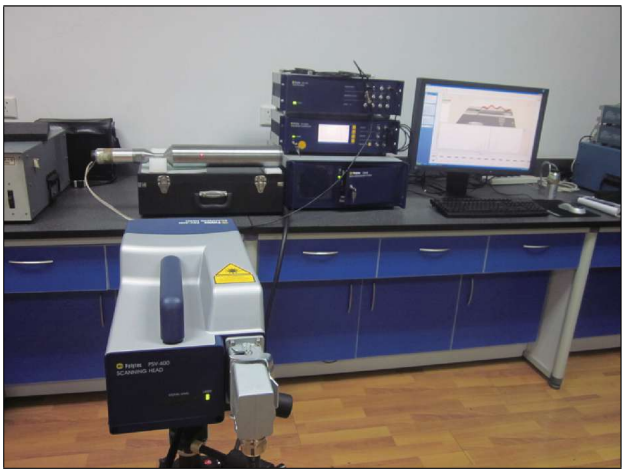


Figure 16. Experimental set-up for the vibrational displacement distribution measurement by using Polytec Laser Scanning Vibrometer.

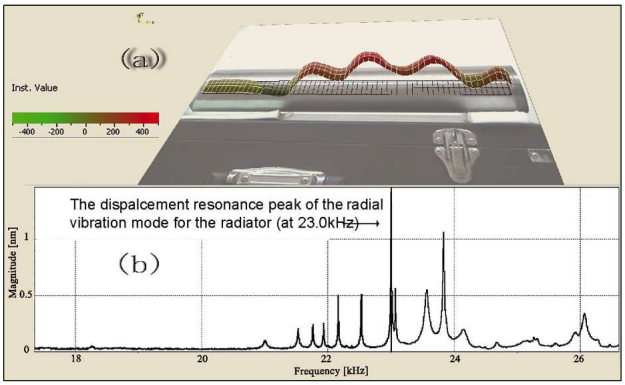


Figure 17. Measured radial vibrational displacement distribution on the side surface of the radiator. (a) Radial displacement field; (b) radial displacement curve of the radiator changing with the frequencies.

the vibrational displacement distribution of the radiator was measured by Polytec PSV-400 Scanning Vibrometer, shown in Figure 16. Finally, we run the radiator in a liquid, as shown in Figure 18.

In Figure 15, (a) is the impedance-frequency curve of the sandwich piezoelectric transducer, and (b) is the impedance-frequency curve of the improved tubular ultrasonic radiator. By comparing Figure 15 with Figure 8, it can be seen that the experimental relationship between the impedance and the frequency is basically the same as the numerically simulated result.

The measured radial vibrational displacement distributions of the radiator are shown in Figure 17. In the figure, the magnitudes of displacement were represented by different colors (red color representing the maximum value of the displacement). It can be seen from Figure 17a that the radial displacement of the radiator is significant. Figure 17b shows the radial displacement curve for the radiator with the frequencies changing from 10 kHz to 30 kHz. It can be seen that there are various resonance peaks in this frequency range and the maximum resonance peak locates at 23.0 kHz. Through observing the radial vibrational displacement distribution of the radiator, apart from the radial vibrational mode (at 23.0 kHz), the other radial flexural vibrational modes (similar as that showed in Figure 9) were also observed. By comparing Figure 17 with Figures 5, 7, and 9c, it can be seen that the measured radial displacement distributions of the tubular radiator are similar as that the simulated ones. The differences can be explained mainly from two factors. One reason is that the standard material parameters used in the simulation are different from the actual values. The other reason is the loss factor of the radiator used in the numerical simulation is not in accordance with the actual value.



Figure 18. The experimental set-up for the tubular radiator drawing about 440 W of power. (a) liquid in the tube; (b) liquid outside of the tube.

The experimental set-up for the radiator operated in a liquid is shown in Figure 18. Considering the maximum power capacitance of the piezoelectric transducer used in the radiator being 500 W, we run this device drawing about 440 W of power when the liquid is in the tube (shown in Figure 18a) and outside of the tube (shown in Figure 18b), respectively. By comparing the cavitations observed in the two cases, the cavitation in the tube is more intense than that outside of the tube. The reasons can be explained as: Firstly, the ultrasound in the tube comes from two sound sources, i.e., the longitudinal vibration of the barbell horn and the radial vibration of the tube. Secondly, the ultrasound radiated by the radial vibration of the tube is focused in the tube. However, the ultrasound outside of the tube is produced only by the radial vibration of the tube, and it is diffused. Therefore, the ultrasound in the tube is more intense than that outside of the tube.

From the above analysis and experimental results, it can be seen that by virtue of the special structure designation and the vibration mode conversion, the radiation surface and displacement amplitude of the radiator can be effectively improved, which is very useful for ultrasonic liquid processing applications. In addition, it should be noted that the cavitation outside of the tube is weaker than that in the tube for the experimental radiator. Thus, in order to get high intensity ultrasound outside of the tube, the vibrational characteristics of the experimental radiator need

to be further improved. Firstly, the power capacitance of a single piezoelectric transducer used in the device is too low to produce an intense ultrasound outside of the tube. It is considered to excite the tubular radiator by both piezoelectric transducer/barbell horn assemblies at both ends of the tube. Secondly, titanium alloy should be used in producing a barbell horn/tube assembly. The advantages of titanium alloy for this purpose are low power losses, good mechanical properties, good corrosion resistance, low density, high strength-to-weight ratio, and fracture toughness. Finally, The value of the electromechanical impedance for the experimental tubular radiator is relatively large, and it can be reduced by improving the machining accuracy of the tubular radiator.

5. Conclusions

This article is dedicated to the design and characterization of a tubular ultrasonic radiator incorporating a piezoelectric transducer/barbell ultrasonic horn assembly. The electro-mechanical equivalent circuit for the tubular ultrasonic radiator in longitudinal and radial composite vibration was given. The resonance frequency, the impedance-frequency curve and the radial vibrational displacement distribution of the radiator were numerically simulated and experimentally measured. The numerical and experimental results validated that, by virtue of the special structure designation and the vibration mode conversion, the radiation surface and displacement amplitude of the radiator can be effectively improved. The tubular ultrasonic radiator can not only be used as a focused ultrasonic radiator when the liquid is processed in the tube, but also be used as radial ultrasonic radiator when the liquid is processed outside of the tube. In addition, it should be noted that, in order to adapt to the practical engineering applications, the vibrational characteristics of the experimental radiator need to be further improved. For example, the power capacitance of the device needs to be further improved; titanium alloy instead of the 45# steel is used in producing a barbell horn/tube assembly; the machining accuracy of the tubular radiator needs to be further improved. It is expected that this kind of radiator can be used in some high power ultrasonic applications, such as ultrasonic liquid processing, ultrasonic extraction, sonochemistry.

Acknowledgement

The author wishes to acknowledge the National Natural Science Foundation of China (11204284) and the Zhejiang Provincial Natural Science Foundation of China (LQ12A04006) for their financial support.

References

[1] J. A. Gallego-Juarez, G. Rodriguez-Corral, L. Gaete-Garreton: An ultrasonic transducer for high power applications in gases. Ultrasonics **16** (1978) 267–271.

[2] J. A. Gallego-Juarez: High-power ultrasonic processing: Recent developments and prospective advances. Physics Procedia **3** (2010) 35–47.

[3] J. A. Gallego-Juarez, G. Rodriguez, V. Acosta, E. Riera: Power ultrasonic transducers with extensive radiators for industrial processing. Ultrasonics Sonochemistry **17** (2010) 953–964.

[4] N. K. Vladimir, S. V. Levin, N. T. Sergey: High power ultrasonic oscillatory systems. 8th International Siberian Workshop and Tutorials EDM 2007, Erlagol, July 1-5, Session V.

[5] S. L. Peshkovsky et al.: Ultrasonic rod waveguide-radiator. United States Patent, No.:7,156,201, 2007.

[6] S. L. Peshkovsky, A. S. Peshkovsky: High-capacity ultrasonic reactor system. International Application Number: PCT/US08/68697, 2008.

[7] S. L. Peshkovsky, A. S. Peshkovsky: Matching a transducer to water at cavitation: Acoustic horn design principles. Ultrasonics Sonochemistry **14** (2007) 314–322.

[8] A. S. Peshkovsky, S. L. Peshkovsky: Acoustic cavitation theory and equipment design principles for industrial applications of high-intensity ultrasound. – In: Book Series: Physics Research and Technology. Nova Science Publishers, Hauppauge, NY, 2010.

[9] O. Dahlem, J. Reisse, V. Halloin: The radially vibrating horn: A scaling-up possibility for sonochemical reactions. Chemical Engineering Science **54** (1999) 2829–2838.

[10] http://www.hielsher.com/ultrasonics/i8000_p.htm.

[11] http://www.crest-ultrasonics.com/push-pull-transducers.

[12] Z. Liang, G. Zhou, Y. Zhang, Z. Li, S. Lin: Vibration analysis and sound field characteristics of a tubular ultrasonic radiator. Ultrasonics **45** (2006) 146–151.

[13] G. Zhou, Z. Liang, Z. Li, Y. Zhang: A tubular focused sonochemistry reactor. Chinese Science Bulletin **52** (2007) 1902–1905.

[14] S. Lin, L. Xu, W. Hu: A new type of high power composite ultrasonic transducer. Journal of Sound and Vibration **330** (2011) 1419–1431.

[15] S. Lin, T. Hua, J. Hu, W. Hu, Z. Fu, L. Xu: High power ultrasonic radiator in liquid. Acta Acustica united with Acustica **97** (2011) 544–552.

[16] S. Lin, S. Wang: Radially composite piezoelectric ceramic tubular transducer in radial vibration. IEEE Transactions on Ultrasonics, Ferroelectrics, and Frequency Control **58** (2011) 2492–2498.

[17] A. Iula, F. Vazquez, M. Pappalardo, J. A. Gallego: Finite element three-dimension analysis of the vibrational behaviour of the Langevin-type transducer. Ultrasonics **40** (2002) 513–517.

[18] L. Xu, S. Lin: Optimization design of high power ultrasonic circular ring radiator in coupled vibration. Ultrasonics **51** (2011) 815–823.